

Physical origin of the large-scale conformity in the specific star formation rates of galaxies

Guinevere Kauffmann

* *Max-Planck Institut für Astrophysik, 85741 Garching, Germany*

5 November 2018

ABSTRACT

Two explanations have been put forward to explain the observed conformity between the colours and specific star formation rates (SFR/M_*) of galaxies on large scales: 1) the formation times of their surrounding dark matter halos are correlated (commonly referred to as “assembly bias”), 2) gas is heated over large scales at early times, leading to coherent modulation of cooling and star formation between well-separated galaxies (commonly referred to as “pre-heating”). To distinguish between the pre-heating and assembly bias scenarios, we search for relics of energetic feedback events in the neighbourhood of central galaxies with different specific star formation rates. We find a significant excess of very high mass ($\log M_* > 11.3$) galaxies out to a distance of 2.5 Mpc around low SFR/M_* central galaxies compared to control samples of higher SFR/M_* central galaxies with the same stellar mass and redshift. We also find that very massive galaxies in the neighbourhood of low SFR/M_* galaxies have much higher probability of hosting radio loud active galactic nuclei. The radio-loud AGN fraction in neighbours with $\log M_* > 11.3$ is four times higher around passive, non star-forming centrals at projected distances of 1 Mpc and two times higher at projected distances of 4 Mpc. Finally, we carry out an investigation of conformity effects in the recently publicly-released Illustris cosmological hydrodynamical simulation, which includes energetic input both from quasars and from radio mode accretion onto black holes. We do not find conformity effects of comparable amplitude on large scales in the simulations and we propose that gas needs to be pushed out of dark matter halos more efficiently at high redshifts.

Key words: galaxies:formation, galaxies:active, galaxies:stellar content, large-scale structure of the Universe

1 INTRODUCTION

The subject of this paper is the physical origin of the very large-scale conformity in the colours and specific star formation rates of isolated central galaxies and their neighbours on scales in excess of 1 Mpc.

The term conformity was first introduced by Weinmann et al (2006) to describe the conformity between the colours of central and satellite galaxies within a single virialized group or dark matter halo. As noted in that paper, there are obvious physical explanations for such effects if they are seen internal to the halo virial radius. In massive dark matter halos, infalling gas is shock heated to temperatures in excess of 10^6 K and then cools over timescales of many gigayears. Cold gas in satellite galaxies moving through a halo can be removed by ram-pressure effects. The combination of ineffi-

cient cooling onto central galaxies, and stripping of gas from satellites could easily produce a conformity effect.

An analysis showing that conformity effects extend well beyond the virial radius for *isolated* central galaxies was first presented in a paper by Kauffmann et al (2013; hereafter K13). In particular, a correlation between the specific star formation rates of red central galaxies with stellar masses less than a few $\times 10^{10} M_\odot$ and the specific star formation rates of their neighbours was found to extend out to scales in excess of 3-4 Mpc. The strength of the effect on large scales was surprisingly large, particularly for low mass galaxies with little ongoing star formation.¹

¹ As seen in Figure 2 of the paper, the median value of SFR/M_* for neighbours of galaxies in the lowest quartile bin in SFR/M_* is depressed by more than a factor of 2 below that measured for neighbours of galaxies in the upper two quartiles, out to distances of at least 3 Mpc.

* E-mail: gamk@mpa-garching.mpg.de

Explaining how correlations in star formation extend out to such large scales is difficult, because this implies some form of causal connection between the history of galaxies in different dark matter halos. This contradicts the assumption that is frequently made in the very simplest halo occupation distribution (HOD) models, namely that the physical properties of a galaxy are determined solely by the mass of the halo in which it resides.

Analysis of N-body simulations has shown that the amplitude of the two-point correlation function of dark matter haloes with masses less than $10^{13} M_{\odot}$ on large scales depends on halo formation time, an effect commonly dubbed “assembly bias” (Gao et al 2005). If the star formation histories of galaxies are correlated with the halo formation time, this could be a possible explanation for the observed large-scale conformity seen in the observations. For this reason, Kauffmann et al (2013) undertook a direct comparison of their observational results with the predictions of the semi-analytic models of Guo et al (2011), which are grafted onto the exact same simulations which were used in the Gao et al analysis of assembly bias. The main conclusion from the comparison was that low amplitude conformity effects were indeed present, but that the amplitude could not match the observational data. Kauffmann et al (2013) then went on to speculate that more exotic effects, e.g. pre-heating of the gas by energy input from active galactic nuclei, might be needed to explain their data.

Since then, a number of theoretical papers have appeared claiming much stronger effects arising from assembly bias alone (Wetzel et al 2014; Hearin et al 2015a,b). The main difference between these models and those of Guo et al (2011) lies in the modelling of supernova feedback effects. In the Guo et al (2011) models, the amount of cold disc gas that is reheated by SN feedback and injected into the hot halo component scales as the fifth power of the circular velocity of the halo. In effect, this implies that the correlation between galaxy star formation history and halo mass will be much stronger than the correlation with halo formation time. Strong scaling in supernova feedback efficiency with halo mass is required to match a number of other observables, such as the slope of the low mass end of the stellar mass function and slope of the stellar mass-metallicity relation at $z=0$. The models of Wetzel et al and Hearin et al do not take into account these additional constraints.

In this paper, we will try to make further progress by analyzing the observed conformity effect in more detail. To distinguish between the pre-heating and the assembly bias scenarios, we propose the following test. We ask whether we can find any evidence for “relics” of present or past energetic feedback events in the vicinity, but outside the host halos of low SFR/M_{*} galaxies. Such relics should not be detected in the vicinity of higher SFR/M_{*} galaxies of the same stellar mass and redshift. We will show that relics in the form of an excess of very high mass ($\log M_{*} > 11.3$) galaxies are found out to a projected distance of 2.5 Mpc from passive low mass galaxies. A significantly larger fraction of these relics *currently* host radio-loud active galactic nuclei. Finally, we carry out an investigation of conformity effects in the recently publicly-released Illustris cosmological hydrodynamical simulation (Vogelsberger et al 2014), which include energetic input both from quasars and radio mode

accretion onto black holes. A Hubble constant $H_0 = 70 \text{ km s}^{-1}$ is adopted throughout the paper.

2 NEW CONSTRAINTS FROM SLOAN DIGITAL SKY SURVEY DATA

We begin with the same volume-limited sample of 11,673 galaxies with $\log M > 9.25$ and redshifts in the range $0.017 < z < 0.03$ as in K13. The upper limit in redshift ensures that we are able to detect all galaxies down to a limiting stellar mass of $2 \times 10^9 M_{\odot}$, irrespective of the intrinsic colour of the system. Galaxies with mass M are defined to be central galaxies if there is no other galaxy with with stellar mass greater than $M/2$ within a projected radius of 500 kpc and with velocity difference less than 500 km s^{-1} . There are 7712 galaxies in our catalogue with stellar masses greater than $5 \times 10^9 M_{\odot}$ to which we can apply this criterion.

For the current analysis, we select a set of passive sub- L_{*} central galaxies in the stellar mass range $9.75 < \log M_{*} < 10.25$ (i.e. similar in mass to the Large Magellanic Cloud) that have SFR/M_{*} values in the lowest quartile of the distribution. The star formation rates we use are the *global* SFR values derived using the methodology outlined in Brinchmann et al (2004). The stellar masses are drawn from the MPA/JHU Data Release 7 value-added catalogue (<http://www.mpa-garching.mpg.de/SDSS/DR7/>). For each of these galaxies, we select four control galaxies closely matched in stellar mass and redshift, but with SFR/M_{*} in the upper two quartiles. These galaxies form our control sample. In Figures 1-4 in this section, results for the passive galaxies are shown in red, while results for the control galaxies are shown in black.

The top two panels of Figure 1 show the cumulative total stellar mass in neighbours as a function of projected radius around central galaxies in two stellar mass ranges, $9.75 < \log M_{*} < 10$ and $10 < \log M_{*} < 10.25$. All neighbours are required to have projected velocity differences less than 500 km s^{-1} from the systemic velocity of the central galaxy. The effect of our isolation cut to define central objects is seen as a break in the slope of the cumulative mass profile at $R = 0.5 \text{ Mpc}$. Here, and everywhere else in the paper, error bars are computed by bootstrap resampling the central galaxy samples. The cumulative stellar mass in neighbours around passive centrals is significantly higher than around the control sample, but note that the difference is less than 0.2 dex in $\log M_{*}$ at all projected radii. The bottom two panels show the cumulative mass in black holes in the neighbours. We estimate black hole mass from the measured velocity dispersion of the galaxy using the formula in Tremaine et al (2002) $\log(M_{\text{BH}}/M_{\odot}) = \alpha + \beta(\sigma/\sigma_0)$, with $\alpha = 8.13$ and $\beta = 4.02$.² As can be seen, the cumulative mass in black holes in the vicinity of the passive centrals is the same as that around the control galaxies.

Next, Figure 2 shows the distribution of the stellar masses of neighbours in three radial bins centred at $R=630 \text{ kpc}$, $R=1.25 \text{ Mpc}$ and $R=2.5 \text{ Mpc}$. Each bin has width 0.5

² The wavelength resolution of the SDSS spectrograph means that velocity dispersions below 70 km/s cannot be reliably determined. In our analysis we simply set the black hole mass to zero in galaxies with $\sigma < 70 \text{ km/s}$

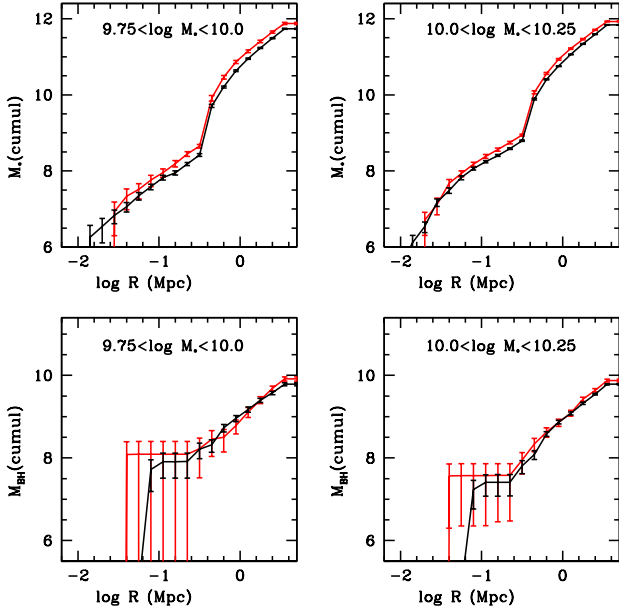


Figure 1. Top: The cumulative total stellar mass in neighbours as a function of projected radius around central galaxies in two stellar mass ranges, $9.75 < \log M_* < 10$ and $10 < \log M_* < 10.25$. The red curves show results for passive centrals; the black curves show results for the control sample of central galaxies. **Bottom:** The cumulative total black hole mass as a function of projected radius around central galaxies.

in $\Delta \log R$. Note that all three of these radial bins lie outside a projected radius of 500 kpc, i.e. the outer radius used for the isolation criterion that defines our central galaxy sample. We see that red central galaxies are more likely to have a very massive neighbour with a stellar mass greater than $2 - 3 \times 10^{11} M_\odot$ than the control central galaxies. This excess is strongest in the closest ($R=630$ kpc) bin, but remains significant out beyond 1.25 Mpc.

We now investigate whether peculiarities exist in the *structural* properties of the neighbours in the vicinity of passive galaxies with low stellar masses. To do this, we convert the *g* and *i*-band surface brightness profiles of each neighbouring galaxy into a stellar mass density profile. The procedure for doing this is described in Kauffmann et al (2007). The SDSS *frames* pipeline extracts an azimuthally-averaged radial surface brightness profile for each galaxy. In the catalogs, this is given as the average surface brightness in a series of annuli, from which interpolated colour and stellar mass density profiles can be derived. The conversion between *g*–*i* colour and *i*-band mass-to-light ratio is given by the relation shown in Figure 15 of Kauffmann et al (2007).

In Figure 3, we show how the total stellar mass in in neighbours around passive central galaxies and the control sample is partitioned as a function of *local* stellar mass surface density. Results are shown for the same three radial bins as in Figure 2. No significant difference is seen in the stellar mass density distribution functions for passive centrals and control galaxies. We conclude that the main distinguishing feature of the population of galaxies in the neighbourhood

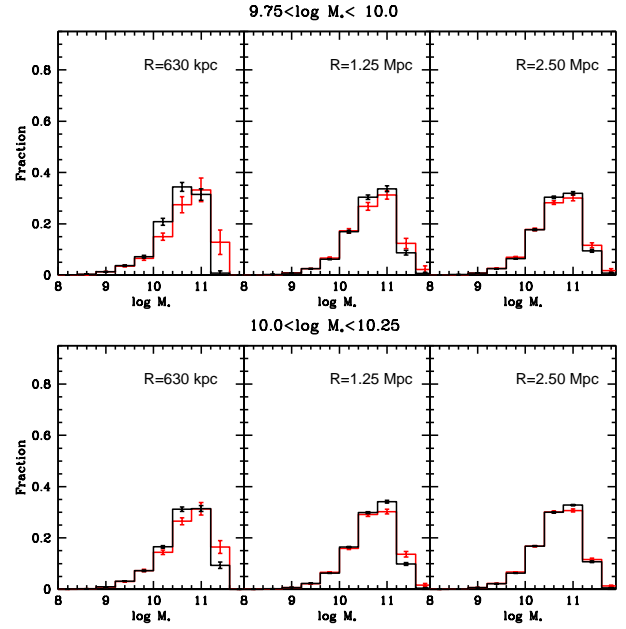


Figure 2. The distribution of the stellar masses of neighbours in three radial bins centred at $R=630$ kpc, $R=1.25$ Mpc and $R=2.5$ Mpc. Results are shown for the stellar mass ranges, $9.75 < \log M_* < 10$ (top) and $10 < \log M_* < 10.25$ (bottom). The red histograms show results for passive centrals; the black histograms show results for the control sample of centrals.

of passive, low mass centrals, is the more probable presence of a giant galaxy with $\log M_* > 11.3$.

2.1 Radio-loud AGN fraction

Best et al (2005) showed that the fraction of galaxies that host radio-loud AGN is a strong function of stellar mass, rising from values close to zero at $10^{10} M_\odot$ to 30% at $M_* = 5 \times 10^{11} M_\odot$. In follow up work, Best et al (2007) also showed that at fixed mass, central galaxies in groups and clusters had higher probability of being radio loud than galaxies of the same mass selected independent of their environment. The difference in radio-loud fraction was largest for low mass galaxies (a factor 10 at $M_* \sim 3 \times 10^{10} M_\odot$), but negligible for the highest mass galaxies (almost no difference for galaxies with masses greater than $3 \times 10^{11} M_\odot$).

In Figure 4, we plot the cumulative fraction of neighbouring galaxies interior to a projected radius R that host radio-loud AGN. Results for neighbours with $\log M_* > 11$ are shown as dotted lines, and for neighbours with $\log M_* > 11.3$ are shown as solid lines. Red lines are for passive centrals and black lines are for the control sample. Radio AGN are identified using the most recent release of a catalogue of 18,286 systems constructed by combining the seventh data release of the Sloan Digital Sky Survey with the NRAO (National Radio Astronomy Observatory) VLA (Very Large Array) Sky Survey (NVSS) and the Faint Images of the Radio Sky at Twenty centimetres (FIRST) survey (Best & Heckman 2012).

As can be seen, the fraction of radio-loud AGN hosted by massive neighbours is significantly higher around the pas-

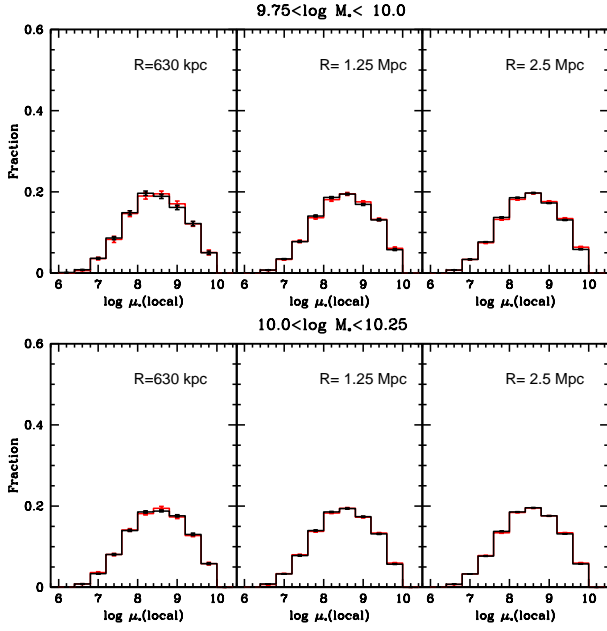


Figure 3. The distribution of the total stellar mass in neighbours as a function of local stellar mass surface density. Results are shown for the same three radial bins and the same stellar mass bins as in Figure 2.

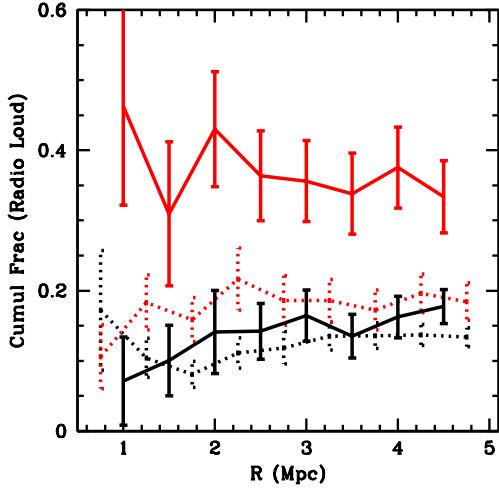


Figure 4. The cumulative fraction of neighbouring galaxies interior to radius R that host radio-loud AGN. Results for neighbours with $\log M_* > 11$ are shown as dotted lines, and for neighbours with $\log M_* > 11.3$ are shown as solid lines. Red lines are for passive centrals and black lines are for the control sample.

sive centrals than it is around the control sample. In contrast to the trends found for central galaxies by Best et al (2007), the *difference is largest for the most massive neighbours*. The excess in radio-loud AGN fraction also appears to extend out to very large radii. Among neighbours with $\log M_* > 11.3$, the difference in radio-loud fraction between



Figure 5. Optical images of six examples of very massive ($\log M_* > 11.3$) galaxies that host radio-loud AGN and that are found within a projected radius $R < 5$ Mpc from a passive low mass central galaxy with velocity difference $\Delta V < 500$ km/s.

the passive centrals and the controls is a factor of 4 at $R=1$ Mpc and is still very significant (a factor of 2) at $R=4$ Mpc.

We conclude that passive low mass central galaxies have high probability of marking the location of patches of the Universe extending over many Mpc where there is a clear excess of massive galaxies hosting radio-loud AGN. Figures 5 and 6 show six examples of such massive relics located within a projected radius of 5 Mpc from a low SFR/M_* central galaxy and with velocity difference $\Delta V < 500$ km/s. Optical images from the SDSS Skyserver are displayed in Figure 5 and radio continuum cut-out images from the FIRST/VLA Image Cutout server are displayed in Figure 6. The optical images show that the massive galaxies are all normal giant ellipticals, with red colours and featureless morphologies. The radio morphologies of the AGN are quite varied – some are compact and unresolved, while others extend over several arcminutes in diameter and exhibit clear double-lobed structures. The most extended of the sources (middle bottom panel) has a physical diameter of 70 kpc. In this case, the radio jets do extend outside the optical radius of the host galaxy. Nevertheless, it is clear from these images that these jets are not currently dumping energy over scales of many Megaparsecs. We speculate instead that much of the gas in the halos of these systems was heated and expelled at early epochs during the formation of the massive galaxy itself, and that the current radio-loud AGN activity simply acts to prevent gas from re-cooling, and to maintain the galaxy in a passive state, similar to what is seen in present-day clusters (see Fabian (2012) for a review).

3 COMPARISON WITH ILLUSTRIS SIMULATION

As discussed in Section 1, Kauffmann et al (2013) compared their observational results with the semi-analytic models of Guo et al (2011). They selected central galaxies and neighbours in the same way as in the observations and found that

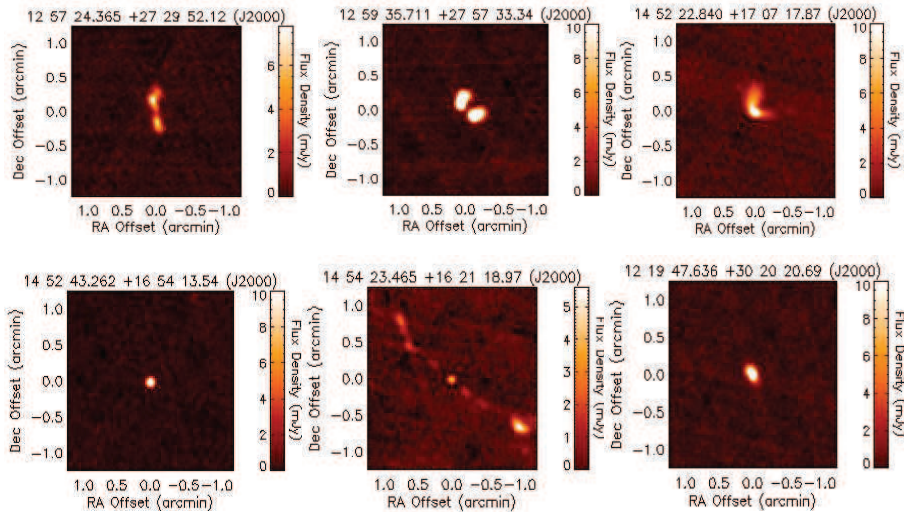


Figure 6. 1.4 GHz radio continuum images of six examples of very massive ($\log M_* > 11.3$) galaxies that host radio-loud AGN and that are found within a projected radius $R < 5$ Mpc from a passive low mass central galaxy with velocity difference $\Delta V < 500$ km/s.

conformity effects on large scales were too weak to match observations. We note that there is no “cross-talk” between gas-physical processes in different dark matter halos in these models. Even though supernovae may eject gas out of the dark matter halo, this gas is simply held in limbo in a so-called ejected reservoir which will eventually re-join the same dark matter halo after a fixed delay. In more recent work, Henriques et al (2013) propose that these re-incorporation times need to be longer in lower mass halos in order to match observed constraints on the evolution of the galaxy mass function at low stellar masses. In these circumstances, the assumption that the baryon reservoir of a halo is always tied to that halo over all cosmic time, is even more contrived.

In numerical hydrodynamical simulations, the thermodynamic evolution of the gas is followed in a self-consistent way. Recently, the Illustris simulation project has publicly released a suite of large volume, cosmological hydrodynamical simulations run with the moving-mesh code Arepo (Nelson et al 2015). The simulations include a complex set of prescriptions for following a whole set of physical processes relevant for the formation and evolution of galaxies (Vogelsberger et al. 2014). In particular, detailed prescriptions for energetic feedback from black holes by quasars triggered during galaxy-galaxy mergers and by bubbles of hot gas produced by radio-loud AGN when black holes accrete at low rates (Sijacki et al 2007; 2015) are included in the simulation code. The Illustris simulation has been demonstrated to provide much better match to basic galaxy properties such as the stellar mass function and stellar mass/halo mass relation than was typical of previous generations of simulations. It thus serves as a useful benchmark for comparisons with a wide variety of different observational data.

In this section, we will carry out two direct comparisons between our SDSS data and Illustris: 1) We will select

a set of isolated central galaxies from the simulation using the same procedure that we use for the observations, and we will ask whether the distribution of specific star formation rates matches what is seen in the observational data. The reason for carrying out the comparison using central galaxies rather than all galaxies, is to separate the effects of internal processes that regulate star formation in isolated galaxies (i.e. supernova and AGN feedback) from the effects of environmental processes such as ram-pressure stripping of gas in group and cluster environments. 2) We examine whether conformity between the colours of the central galaxies and those of their neighbours is seen at separations larger than 1 Mpc.

3.1 Specific star formation rate distributions of isolated central galaxies

We extract x, y, z positions, velocities, stellar masses and star formation rates for galaxies in the $z=0$ SUBFIND subhalo catalog (see Nelson et al. (2015) for more details). We adopt stellar masses and star formation rates measured within twice the half mass radius to derive our fiducial measures of SFR/M_* and we consider only those subhalos containing galaxies with stellar masses greater than $2 \times 10^9 M_\odot$. We select isolated central galaxies the same way as in the data, by requiring that no other galaxy more massive than half the mass of the object be found within a radius $dr = \sqrt{dx^2 + dy^2}$ less than 500 kpc and within a velocity difference $H_0 dz + (dv_z)$ less than 500 km/s.

Figure 7 shows histograms of SFR/M_* for galaxies in three different bins of stellar mass: $9.75 < \log M_* < 10$, $10.75 < \log M_* < 11$, and $11.25 < \log M_* < 11.5$. The upper panels show results for the SDSS, while the lower panels show results for Illustris. In order to illustrate the systematic

uncertainties arising from the aperture within which we measure SFR/M_* , we plot distributions for SFR/M_* measured within the 3 arcsec fibre aperture as dotted histograms in the upper panels. In the lower panels, the dotted histograms are for SFR/M_* measured within the radius containing half the stellar mass. Independent of which measure of SFR/M_* is adopted, significant discrepancies between the simulations and the data are apparent:

(i) In the lowest mass bin, there is a significant tail of galaxies with $\log SFR/M_* < -11$, which is missing in the Illustris simulation. The SFR/M_* values of the simulated galaxies are all peaked in a very narrow range around $\log SFR/M_* \sim -10$, which implies that these galaxies have formed stars at a constant rate over the age of the Universe.

(ii) In the bin with $10.75 < \log M_* < 11$, we see that the bulk of the population in the SDSS have low SFR/M_* , whereas the opposite is true in Illustris.

(iii) In the highest mass bin, essentially all galaxies in SDSS are passive with $\log SFR/M_* < -11$, but Illustris has a much larger fraction of galaxies which are still actively forming stars.

We note that Sparre et al (2015) carried out a comparison of only the star-forming “main sequence” with observational data at different redshifts, and did not note the discrepancy in passive galaxy fractions as a function of stellar mass at $z = 0$.

Our main conclusion, therefore, is that star formation quenching processes appear to work too inefficiently in Illustris compared to the real Universe. We will speculate on reasons why this might be the case in the final section.

3.2 Evidence for conformity?

Given that the tail of passive low mass galaxies seen in SDSS data is not present in the Illustris simulation and that high mass galaxies form stars at rates that are too high compared with observations, one might question the validity of carrying out a conformity analysis. Nevertheless, in view of the different predictions for the effect of assembly bias on the colours and star formation rates of galaxies in the literature, we feel that it is useful to examine conformity effects in a numerical hydrodynamical simulation that was not explicitly tuned to reproduce this effect.

Figure 8 shows the specific star formation rates of neighbouring galaxies as a function of projected radius around $3 \times 10^9 - 10^{10} M_\odot$ central galaxies in the lowest 25th percentile bin in SFR/M_* (red lines) and in the 50th-75th percentile bin (black lines). Solid lines show the median SFR/M_* of the neighbours, while dashed and dotted lines show the 25th and 75th percentiles of the SFR/M_* distribution. The left panel shows results for galaxies from the Sloan Digital Sky Survey. We now plot our results over the projected radius range 1-30 Mpc and we find that the effect appears to persist out to a radius of ~ 10 Mpc in this mass bin. Results for Illustris are plotted in the right panel.

The first-order discrepancy in the *dynamic range* in SFR/M_* spanned by neighbouring galaxies is again very apparent. Similar to what was found for the Guo et al (2011) semi-analytic models, the depression in star formation rate around passive centrals in Illustris at projected radii larger

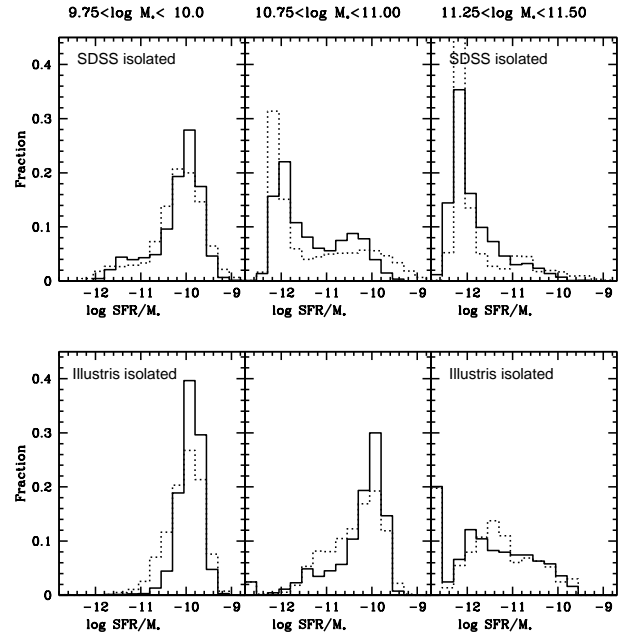


Figure 7. Histograms of SFR/M_* for central isolated galaxies in three different bins of stellar mass: $9.75 < \log M_* < 10$, $10.75 < \log M_* < 11$, and $11.25 < \log M_* < 11.5$. The upper panels show results for the SDSS, while the lower panels show results for Illustris. In the top panels, the solid histograms are for the global SFR/M_* measurements from the MPA/JHU catalogue (see Brinchmann et al. (2004) for details), while dotted histograms are for SFR/M_* measured within the 3 arcsec SDSS fibre. In the bottom panels, the solid histograms are for SFR/M_* measured within twice the half mass radius of the main galaxy of the subhalo (see Nelson et al. (2015) for details), while dotted histograms are for SFR/M_* measured within the half mass radius.

than 1 Mpc is very small and is mainly confined to the lowest 25th percentile of the SFR/M_* distribution.

4 SUMMARY AND DISCUSSION

In this paper, we have attempted to further our understanding of the large scale correlations between the specific star formation rates in isolated low mass galaxies and their distant neighbours. In particular, we test the hypothesis that energetic feedback from an early generation of accreting black holes may be responsible for heating gas to high temperatures over large scales. We find an excess number of very massive galaxies out to a radius of 2.5 Mpc around passive central galaxies. In addition, we find that the probability for these massive galaxies to host radio loud AGN at the present day is 3-4 times higher compared to massive neighbours around the control sample. Interestingly, this radio AGN excess extends out to projected radii beyond 5 Mpc. We have compared our results to the Illustris simulation, which includes energetic feedback by both a quasar and radio galaxy population, but do not find conformity effects of comparable strength to those seen in the data.

Recent work by Choi et al (2015) has highlighted how different prescriptions for AGN feedback can have profound

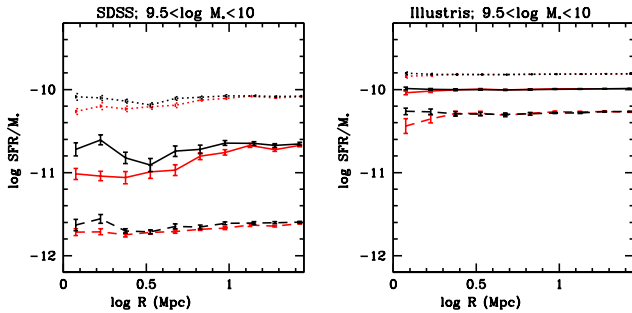


Figure 8. The specific star formation rates of neighbouring galaxies is plotted as a function of projected radius around $3 \times 10^9 - 10^{10} M_{\odot}$ central galaxies in the lowest 25th percentile bin in SFR/M_* (red lines) and in the 50th-75th percentile bin in SFR/M_* (black lines). Solid lines show the median SFR/M_* of the neighbours, while dashed and dotted lines show the 25th and 75th percentiles of the SFR/M_* distribution. The left panel shows results for galaxies from the Sloan Digital Sky Survey, while the right panel is for Illustris.

effect on the properties of the gas around massive ellipticals. By switching from a thermal feedback prescription similar to the one used in the Illustris simulation to a mechanical and radiation feedback model that operates during high black hole accretion rate growth phases, the X-ray luminosities of massive ellipticals are found to decrease by a factor of 10-100, because much more of the gas is blown out beyond the halo virial radius, providing a much better fit to the observed X-ray luminosities of elliptical galaxies at the present day.

Bahé & McCarthy (2013) have used cosmological hydrodynamical simulations to show that direct ram pressure interaction with an extended gas ‘halo’ surrounding massive galaxies can be sufficiently strong to strip the gaseous atmospheres of infalling galaxies out to distances of up to 5 virial radii. We might also even speculate that the extended hot gas left over from an early violent gas ejection event forms a reservoir that is able to fuel black holes at low rates and trigger radio-mode AGN at later epochs. These radio-loud AGN in turn prevent gas from cooling efficiently, leading to large, coherent zones of the Universe where galaxies can no longer form any stars.

Recent observational evidence that gas has been expelled from a substantial number of massive studies has come from studies of the X-ray emission from from 250 000 “locally brightest galaxies” selected from the Sloan Digital Sky Survey by Anderson et al (2015). These authors apply the same cut employed in this paper to select central galaxies and then stack X-ray data from the ROSAT All-Sky Survey to recover the mean X-ray luminosity as a function of galaxy mass down to $M_* = 10^{10.8} M_{\odot}$. Interestingly, the relation they infer between X-ray luminosity and dark matter halo mass has normalization more than a factor of 2 below relations that have been derived based on X-ray-selected cluster samples. This suggests that there is a lot of intrinsic scatter between X-ray luminosity and halo mass. The authors speculate that one explanation for this scatter is that gas has been pushed outwards in the low luminosity systems. High sensitivity maps of hot gas in wide range of different environments using next-generation facili-

ties such as the eROSITA telescope will be needed to make further progress on this topic. It is currently necessary to stack thousands of galaxies in ROSAT to recover a signal, but eROSITA should enable similar analyses for individual galaxies, or for smaller stacked samples, allowing us to pinpoint the conditions under which gas is confined within dark matter halos and the conditions that lead to its expulsion.

It remains to be seen whether changes to AGN feedback prescriptions in Illustris will be sufficient to bring the specific star formation rate distributions of simulated galaxies into better agreement with observations. Sparre et al (2015) demonstrate that there are too few strongly starbursting galaxies in the simulation and propose that the fixed, stiff equation of state used to describe the interstellar medium may require modification. The fact that virtually all low mass galaxies in the simulation have $SFR/M_* \sim -10$ suggests that the interstellar medium does not respond very sensitively to the dynamical history of the galaxy. In contradiction with the written claims in their paper, Figure 1 of Sales et al (2015) reveals rather poor agreement between the density profiles of blue and red satellite galaxies in Illustris and SDSS. In particular, the differences between the profiles for blue and red galaxies are larger for low mass galaxies in SDSS, but the *opposite* is seen in the simulations. Further comparisons with the EAGLE simulations, which have similar resolution and claim even better agreement with the stellar mass function and the $M_* - M_{halo}$ relation (Schaye et al 2015), but which include very different implementation of much of the galaxy formation physics, will be useful for generating improvements to the next generation of simulations.

ACKNOWLEDGMENTS

I thank Aaron Bray for helpful discussions. Thank you to the Aspen Center for Physics and the NSF Grant No. 1066293 for hospitality and supporting minds during the analysis phase and writing of this paper.

REFERENCES

- Anderson M. E., Gaspari M., White S. D. M., Wang W., Dai X., 2015, MNRAS, 449, 3806
- Bahé Y. M., McCarthy I. G., Balogh M. L., Font A. S., 2013, MNRAS, 430, 3017
- Best P. N., Kauffmann G., Heckman T. M., Brinchmann J., Charlot S., Ivezić Ž., White S. D. M., 2005, MNRAS, 362, 25
- Best P. N., von der Linden A., Kauffmann G., Heckman T. M., Kaiser C. R., 2007, MNRAS, 379, 894
- Best P. N., Heckman T. M., 2012, MNRAS, 421, 1569
- Brinchmann J., Charlot S., White S. D. M., Tremonti C., Kauffmann G., Heckman T., Brinkmann J., 2004, MNRAS, 351, 1151
- Choi E., Ostriker J. P., Naab T., Oser L., Moster B. P., 2015, MNRAS, 449, 4105
- Fabian A. C., 2012, ARA&A, 50, 455
- Gao L., Springel V., White S. D. M., 2005, MNRAS, 363, L66
- Guo Q., et al., 2011, MNRAS, 413, 101

- Hearin A. P., Behroozi P. S., van den Bosch F. C., 2015, arXiv, arXiv:1504.05578
- Hearin A. P., Watson D. F., Bosch F. C. v. d., 2015, MNRAS, 452, 1958
- Henriques B. M. B., White S. D. M., Thomas P. A., Angulo R. E., Guo Q., Lemson G., Springel V., 2013, MNRAS, 431, 3373
- Kauffmann G., et al., 2007, ApJS, 173, 357
- Kauffmann G., Li C., Zhang W., Weinmann S., 2013, MNRAS, 430, 1447
- Nelson D., et al., 2015, arXiv, arXiv:1504.00362
- Sales L. V., et al., 2015, MNRAS, 447, L6
- Schaye J., et al., 2015, MNRAS, 446, 521
- Sijacki D., Springel V., Di Matteo T., Hernquist L., 2007, MNRAS, 380, 877
- Sijacki D., Vogelsberger M., Genel S., Springel V., Torrey P., Snyder G. F., Nelson D., Hernquist L., 2015, MNRAS, 452, 575
- Sparre M., et al., 2015, MNRAS, 447, 3548
- Tremaine S., et al., 2002, ApJ, 574, 740
- Vogelsberger M., et al., 2014, MNRAS, 444, 1518
- Weinmann S. M., van den Bosch F. C., Yang X., Mo H. J., 2006, MNRAS, 366, 2
- Wetzell A. R., Tinker J. L., Conroy C., Bosch F. C. v. d., 2014, MNRAS, 439, 2687